发 光 学 报
CHINESE JOURNAL OF LUMINESCENCE

Article ID: 1000-7032(XXXX)XX-0001-12

Luminescent properties of $Ca_5Ga_6O_{14}:Eu^{2+}$ and its application to warm white LEDs

Kang Mengyi[1], Wang Dawei[2], Zhao Jinxin[2], Wang Zhijun[1*], Han Xuping[1], Zhang Guodong[1], Suo Hao[1], Yang Zhiping[1], Li Panlai[1*]

(1. *Hebei Key Laboratory of Optic-electronic Information and Materials, College of Physics Science & Technology, Hebei University, Baoding* 071002, *PR China*;
2. *Hebei Key Laboratory of Semiconductor Lighting and Display Critical Materials, Hebei Ledphor Optoelectronics Technology Co., LTD. Baoding*, 071000, *PR China*)

* *Corresponding Authors, E-mail: wangzj*1998@126.*com, li_panlai*@126.*com*

Abstract: Eu^{2+} can be excited by a broad blue light band and exhibits characteristics of broad wavelength emission. Due to the significant influence of the crystal field environment on Eu^{2+} ions, selecting appropriate host materials or adjusting host components can regulate the emission properties of Eu^{2+}. This approach also enables the phosphor to be highly compatible with blue light chips, compensating for the red spectral deficiency in commercial white LEDs and enhancing the lighting quality of white LEDs. This study selected the gallate $Ca_5Ga_6O_{14}$ as the matrix and synthesized Eu^{2+}-doped red phosphor via a high temperature solid-state method. The luminescence properties were optimized by employing an Al^{3+} ion substitution strategy to replace Ga^{3+} cations in the host, and the quantum efficiency can reach 79.2%, and the luminous intensity at 423 K attained 60% of room temperature. By integrating the $Ca_5Ga_{5.8}Al_{0.2}O_{14}:0.01Eu^{2+}$ red phosphor with the commercial yellow phosphor $Y_3(Al, Ga)_5O_{12}:Ce^{3+}$ and a blue light chip, a white LED device was fabricated, which exhibits a color rendering index (CRI) of 95.5 and a correlated color temperature (CCT) of 4002 K. This demonstrates the promising application prospects of the red phosphor in the field of white light LEDs.

Keywords: Eu^{2+}; red phosphor; oxide; white light emitting diodes

CLC number: **Document code**:

DOI: 10.37188/CJL.20260044 **CSTR**: 32170.14.CJL.20260044

暖白光LEDs用$Ca_5Ga_6O_{14}$: Eu^{2+}荧光粉的发光特性

康梦伊[1], 王大伟[2], 赵金鑫[2], 王志军[1*], 韩旭平[1], 张国栋[1], 索 浩[1], 杨志平[1], 李盼来[1*]

(1.河北大学,河北省光电信息材料重点实验室,物理科学与技术学院, 河北 保定 071002;
2.河北省半导体照明与显示关键材料重点实验室, 河北 保定 071000)

摘要: Eu^{2+}可被宽蓝光带激发,并表现出宽波长发射特性。由于Eu^{2+}离子受晶体场环境影响较大,通过选择合适的基质或者调控基质组分可以调控Eu^{2+}的发光性能,且激发带与蓝光芯片发射高度匹配,用以补充商用白光LED的红色光谱缺失,提高白光LED的照明质量。以镓酸盐$Ca_5Ga_6O_{14}$为基质,通过高温固相法合成了Eu^{2+}掺杂红色荧光粉,利用Al^{3+}离子取代基质中Ga^{3+}离子的调控策略优化其发光性能,量子效率可达79.2%,而且在423K温度下的发光强度达到室温时的60%。将$Ca_5Ga_{5.8}Al_{0.2}O_{14}:0.01Eu^{2+}$红光荧光粉与商用黄绿色荧光粉$Y_3$

收稿日期: XXXX-XX-XX; **修订日期**: XXXX-XX-XX
基金项目: 国家自然科学基金(51902080)
National Natural Science Foundation of China (No.51902080).

$(Al, Ga)_5O_{12}:Ce^{3+}$及蓝光芯片集成,所得白光LEDs器件的显色指数为95.5,相关色温为4002 K。这表明材料在暖白光LEDs方面有一定的应用潜力。

关 键 词: Eu^{2+}; 红色荧光粉; 氧化物; 白光发光二极管

1 Introduction

Currently, commercial white LEDs primarily utilize yellow phosphor YAG: Ce^{3+} combined with blue LEDs to achieve white light[1]. However, the resulting white light spectrum lacks red components, typically yielding a color rendering index (CRI) of 70-80[2,3]. This results in mediocre color reproduction and limits application scenarios. Furthermore, due to the high blue light component, the color temperature predominantly falls within the cool white spectrum (above 5000 K). This emits light harmful to the human eye, failing to achieve a deep integration of lighting and health. Red phosphors play a crucial role in achieving high-quality warm white lighting in white LEDs. However, currently available commercial red phosphors are mainly limited to nitride and fluoride systems such as $CaAlSiN_3$[4], $Sr_2Si_5N_8$[5] and K_2SiF_6[6]. Nitride red phosphors face high preparation costs and stringent conditions. The use of corrosive HF in $K_2SiF_6:Mn^{4+}$ synthesis also causes serious environmental and health issues, hindering their large-scale application against the trend of green development. [7,8]. Compared to nitrides and fluorides, oxides stand out due to their advantages of simple synthesis processes, low cost, environmental friendliness, and rich structural diversity[9].

Among currently reported blue-light-excitable red phosphors, materials capable of being packaged with commercial yellow phosphors to produce white LEDs with high color rendering index (CRI > 95) and low color temperature (CCT < 4000 K) remain few and far between[10]. In 2021, a $Sr_2Sc_{0.5}Ga_{1.5}O_5:Eu^{2+}$ red phosphor was reported, and its emission wavelength was red-shifted from 614 nm to 728 nm by Ba substitution for Sr. This red $Sr_{1.7}Ba_{0.3}Sc_{0.5}Ga_{1.5}O_5:Eu^{2+}$ phosphor was used to fabricate a white LED device with a color rendering index of 91.1 and a correlated color temperature of 4750 K[11]. In 2022, CaO: Eu^{2+} was reported to exhibit broadband emission at 661 nm under 466 nm blue excitation[12]. White LEDs fabricated with this phosphor achieved a CRI of 91.2 and a CCT of 3435 K, enabling warm white lighting; Li et al. developed a blue-light-excited red phosphor, $BaSrLu_4O_8:Eu^{2+}$, exhibiting high quantum efficiency. White LEDs encapsulated with this phosphor achieved a CRI of 84.4 and a CCT of 4295 K[13]; In 2023, Hu et al. enhanced the luminescence properties of $CaYGaO_4:Eu^{2+}$ via secondary reduction. This phosphor exhibits red light emission centered at 650 nm when excited at 470 nm, enabling the fabrication of white LED devices with a CRI of 89.7 and a CCT of 3780 K[14]. White LEDs encapsulated with the above red materials can achieve warm white illumination, but their CRI values remain below 95, failing to meet high-CRI requirements. This limits their application in lighting scenarios with stringent quality demands. More importantly, LEDs generate heat during operation, which may affect lighting performance[15]. Consequently, there is a need to develop a blue-light-excitable oxide red phosphor with excellent performance that can effectively enhance the relevant parameters of white LEDs.

Eu^{2+} ions are significantly influenced by their crystal field environment[16]. By selecting suitable host environments or adjusting matrix components, it is possible to achieve emission of light with different properties from Eu^{2+}, as well as high compatibility with blue-light excitation chips. Given that Eu^{2+} can be excited by a broad blue light band and exhibits characteristics of broad long-wavelength emission, it holds broad application prospects in compensating for the red light spectrum deficiency in white LEDs to achieve warm white lighting[17]. Eu^{2+} tend to readily emits red light in gallates. In our work, we selected the gallate $Ca_5Ga_6O_{14}$ as the host material [18]. Existing studies on luminescent materials based on $Ca_5Ga_6O_{14}$ mostly focus on luminescence excited by UV radiation and per-

sistent luminescence, with applications mainly concentrated in the field of counterfeit prevention. However, targeting the practical application requirements of commercial blue LED chips, relevant research on red emission excited by blue light in the $Ca_5Ga_6O_{14}$ system doped with Eu^{2+} remains relatively limited. When excited by 468 nm blue light, $Ca_5Ga_6O_{14}:Eu^{2+}$ emits red light with a luminescence center at 650 nm. By substituting Al^{3+} ions for Ga^{3+} ions in the host, the quantum efficiency of the phosphor increased from 17.61% to 79.2%. Diffuse reflectance spectroscopy analysis further confirms that the cation tuning strategy modifies the crystal field environment, leading to enhanced blue-light absorption of the phosphor and a consequent improvement in the phosphor's quantum efficiency. Finally, white LEDs encapsulated with this phosphor exhibited superior performance parameters, significantly enhancing lighting quality.

2 Experimental section

2.1 Materials synthesis

$Ca_5Ga_6O_{14}: Eu^{2+}$ and $Ca_5Ga_{6-y}Al_yO_{14}: 0.01Eu^{2+}$ were synthesized via the high temperature solid state method. The synthesis process employed NH_4Cl as a fluxing agent to optimize the synthesis procedure. The raw materials were $CaCO_3$ (99.99%), Ga_2O_3 (99.99%), Al_2O_3 (99.99%), Eu_2O_3 (99.99%), NH_4Cl (99.99%). Reagent masses were selected according to specific ratios, weighed, and placed into an agate mortar dried in an oven. The mixture was ground at a uniform speed for 30 minutes to ensure thorough blending. The ground mixture was transferred into an alumina crucible, which was then embedded in excessive carbon powder to provide a reducing atmosphere during sintering. To avoid contamination from carbon powder volatilization, the carbon powder was placed outside the sealed crucible without direct contact with the sample. The crucible was heated in a box furnace at a rate of 4 ℃/min to a maximum sintering temperature of 1200 ℃ and held for 240 minutes. After the sintering process is completed, the crucible was cooled to below 70 ℃ before removal. The sintered sample was ground thoroughly in an agate mortar to obtain a white homogeneous powder for further characterization.

2.2 LED lamp fabrication

Adhesive A, Adhesive B, and the required phosphor were weighed in a 1:4:5 mass ratio. After weighing, they were placed in a container and thoroughly mixed using a glass rod. The mixed sample was encapsulated with a blue LED chip, then placed in an oven and baked at 70°C for 2 hours. Finally, a white LED was obtained.

2.3 Materials Characterization

X-ray diffraction (XRD) patterns were measured using a Bruker D8 X-ray diffractometer (XRD) (D8 ADVANCE, Bruker AXS LTD, Germany), with an instrument step size of 0.02° and a diffraction range of 10°-60°. Additionally, Rietveld refinement was performed on the samples using the General Structure Analysis System (GSAS). Morphological features were recorded using a field emission scanning electron microscope (Gemini SEM 360). X-ray photoelectron spectroscopy (XPS) was performed on a Thermo Fisher ESCALAB 250Xi (UK). This instrument operates at an ultimate vacuum of 5×10^{-10} mbar with an energy resolution of 0.45 eV. The materials' photoexcitation (PLE), photoluminescence (PL), temperature-dependent luminescence spectra of phosphors, fluorescence lifetime decay curves, and quantum efficiency were measured. These spectra were obtained using a fully functional steady-state/transient fluorescence spectrometer. This instrument is a FLuorolog-3 model, featuring a 450 W xenon lamp excitation source and an iHR320 detector. The diffuse reflectance spectra of samples were measured using a Hitachi U4100 UV-Vis-NIR spectrometer. The measurements employed $BaSO_4$ as the substrate and covered a scanning range of 200-1200 nm.

3 Results and discussion

3.1 Phase purity and crystal structure

$Ca_5Ga_6O_{14}$ belongs to the orthorhombic space group Cmc21, with lattice parameters a = 11.495 Å, b = 11.270 Å, c = 10.479 Å, and V = 1357.54 Å^3. The crystal structure of $Ca_5Ga_6O_{14}$ is shown in Fig. 1a, Ca^{2+} and Ga^{3+} ions form hexacoordinated octahedra [CaO_6] and tetracoordinated hexahedra [GaO_4], re-

spectively, with surrounding O^{2-} ions. The [CaO_6] group occupies three distinct sites, appearing as two octahedra and one trigonal prism, while the [GaO_4] group adopts a trigonal pyramid configuration [19, 20]. Based on the ionic radius matching rule, the ion radius of Eu^{2+}(r = 0.117 Å, CN = 6) is closer to that of Ca^{2+}(r = 0.1 Å, CN = 6), making Eu^{2+} ions more likely to occupy the Ca^{2+} site rather than the Ga^{3+}(r = 0.062 Å, CN = 6) site in the $Ca_5Ga_6O_{14}$ host. The measured XRD patterns of $Ca_5Ga_6O_{14}$:xEu^{2+}(x = 0-0.02) agree with the standard card data for $Ca_5Ga_6O_{14}$ crystals (PDF#78-1180), as shown in Fig. S1, indicating that Eu^{2+} ion doping introduces no impurities and the synthesized samples are single-phase.

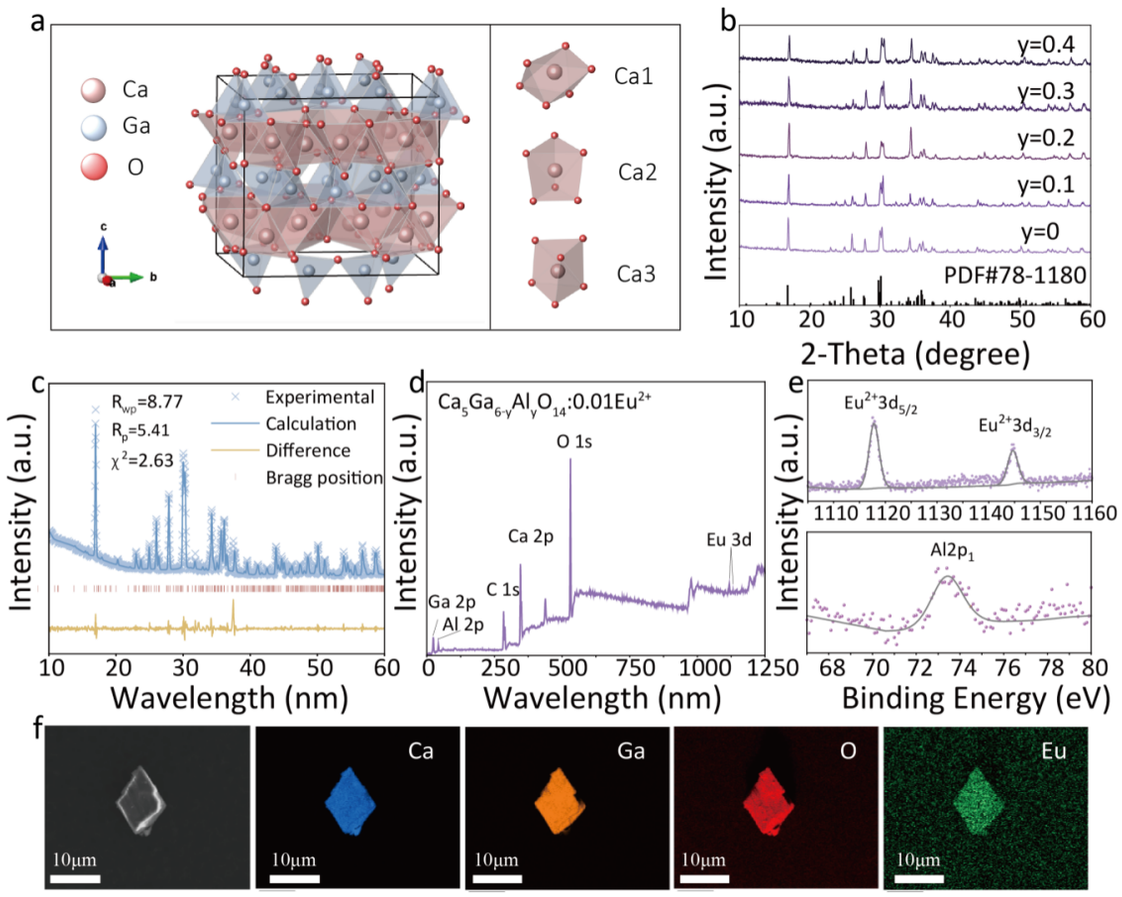

图 1 (a) Ca5Ga6O14 的晶体结构示意图;(b) Ca5Ga6-yAlyO14:0.01Eu2+(y = 0-0.4)的 XRD 图谱;(c) Ca5Ga6O14:0.01Eu2+的精修结果;(d) Ca5Ga6-yAlyO14:0.01Eu2+(y = 0.2)的 XPS 扫描全谱;(e) Eu-3d 能级 XPS 光电子能谱与 Al-2p 能级 XPS 光电子能谱;(f) Ca,Ga,O,Eu 的元素映射图像.

Fig.1 (a) Crystal structure of the $Ca_5Ga_6O_{14}$. (b) XRD pattern of $Ca_5Ga_{6-y}Al_yO_{14}$:0.01Eu^{2+}(y = 0-0.4). (c) Rietveld refinements of $Ca_5Ga_6O_{14}$:0.01Eu^{2+}. (d) XPS survey scan spectra of $Ca_5Ga_{6-y}Al_yO_{14}$:0.01Eu^{2+} (y = 0.2). (e) Eu-3d energy level XPS spectrum and Al-2p energy level XPS spectrum. (f) Element mapping images of Ca, Ga, O, Eu.

Subsequently, Al^{3+} was introduced into $Ca_5Ga_6O_{14}$: 0.01Eu^{2+} to synthesize $Ca_5Ga_{6-y}Al_yO_{14}$: 0.01Eu^{2+} (y= 0-0.4), whose XRD pattern is shown in Fig. 1b. It is observed that Al^{3+} doping did not introduce any impurity phases. Rietveld refinement was performed on $Ca_5Ga_6O_{14}$:0.01Eu^{2+}, with the refined results shown in Fig. 1c. The refinement parameters R_{wp} = 8.77%, R_p = 5.41%, χ^2 = 2.63 fall within reasonable ranges, indicating good crystallinity of the sample. The refined unit cell parameters are listed accordingly in Table S1.

The XPS spectrum of $Ca_5Ga_6O_{14}$: 0.01Eu^{2+} is shown in Fig. S2. Peaks corresponding to Eu, Ca, Ga, O, and other elements were identified, confirming the successful doping of Eu^{2+} into the lattice. Additionally, the XPS spectrum of the doped Eu element in the $Ca_5Ga_6O_{14}$: 0.01Eu^{2+} was tested, as shown in Fig. S3. Two peaks detected in the Eu 3d

orbitals (1144.68 eV and 1117.86 eV) correspond to the binding energy peaks of the Eu^{2+} $3d_{3/2}$ and $3d_{5/2}$ energy levels[21], respectively, confirming that the luminescence in the material originates from Eu^{2+} ions. Fig. 1d shows the full XPS spectrum of $Ca_5Ga_{6-y}Al_yO_{14}$: $0.01Eu^{2+}$ (y = 0.2). Binding energy peaks corresponding to the Ca 2p, O 1s, Ga 2p, and Eu 3d orbital energy levels are all detected in $Ca_5Ga_{6-y}Al_yO_{14}$: $0.01Eu^{2+}$ (y = 0.2). Furthermore, XPS spectra of Al and the dopant Eu ions in the $Ca_5Ga_{6-y}Al_yO_{14}$: $0.01Eu^{2+}$ (y = 0.2) were measured, as shown in Fig. 1e. The binding energy peaks corresponding to the $3d_{3/2}$ and $3d_{5/2}$ levels of Eu^{2+} were detected, indicating luminescence from Eu^{2+} ions in the material. Simultaneously, a peak with a binding energy of 73.44 eV was detected, confirming the successful doping of Al^{3+} to replace Ga^{3+}.

Fig. 1f and Fig. S4 depict the scanning electron microscope (SEM) image of $Ca_5Ga_6O_{14}$: $0.01Eu^{2+}$. The microcrystals exhibit a smooth surface with an average grain size of approximately 10 μm, indicating high crystallinity. Furthermore, the elemental mapping image (EDS) reveals uniform distribution of Ca, Ga, O, and Eu elements throughout the sample, confirming successful synthesis of the phosphor and effective Eu^{2+} doping.

3.2 Luminescent properties

Fig. 2a displays the photoluminescence and excitation spectra of $Ca_5Ga_6O_{14}$: $0.01Eu^{2+}$, along with its corresponding absorption spectrum. Under blue light excitation at 468 nm[21], $Ca_5Ga_6O_{14}$:$0.01Eu^{2+}$ exhibits red light emission centered at 650 nm, originating from the Eu^{2+} $4f^65d^1 \rightarrow 4f^7$ transition[22, 23]. Furthermore, the excitation spectrum at 650 nm reveals a broad excitation band spanning wavelengths from 400 nm to 600 nm, enabling efficient excitation by 468 nm blue light. The absorption spectrum of the sample was measured, with its primary absorption range spanning 400 nm to 600 nm, exhibiting excellent consistency with the excitation spectrum. Fig. 2b displays the emission spectra of $Ca_5Ga_6O_{14}$: xEu^{2+} (x = 0-0.02) under 468 nm blue light excitation. As

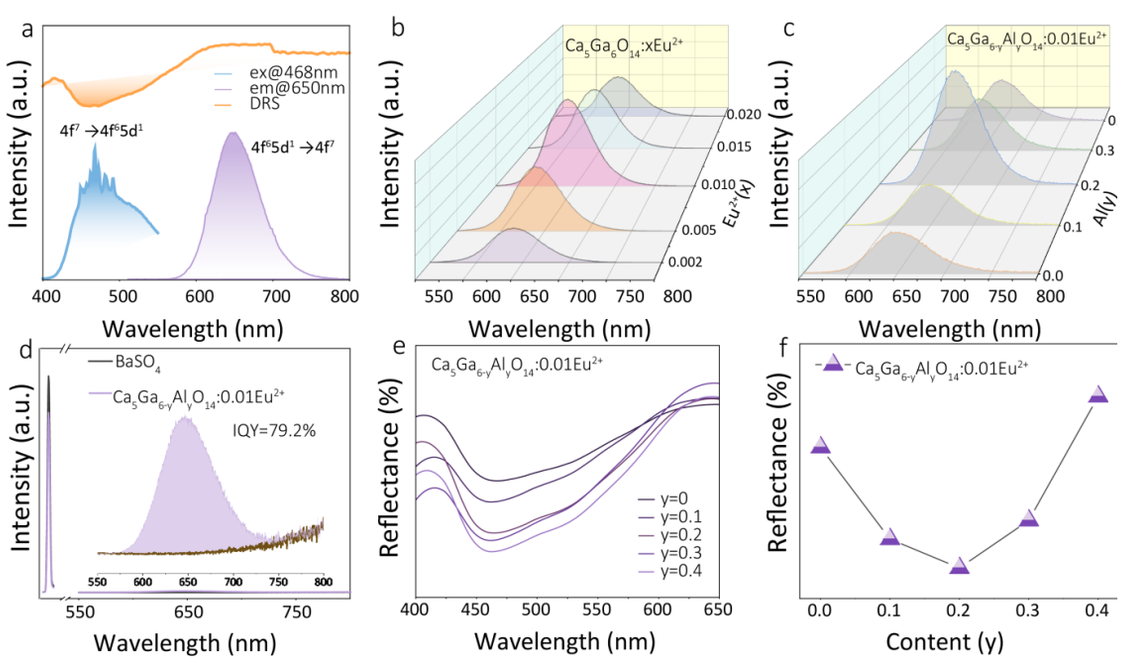

图 2 (a) 室温下 Ca5Ga6O14:0.01Eu2+激发光谱、发射光谱和吸收光谱;(b) Ca5Ga6O14:xEu2+ (x = 0-0.02)的发射光谱;(c) Ca5Ga6-yAlyO14:0.01Eu2+ (y = 0-0.4)的发射光谱;(d) Ca5Ga6-yAlyO14:0.01Eu2+ (y = 0.2)的量子效率;(e) Ca5Ga6-yAlyO14:0.01Eu2+ (y = 0-0.4)的漫反射吸收光谱;(f) Ca5Ga6-yAlyO14:0.01Eu2+ (y = 0-0.4)的蓝光吸收特性。

Fig.2 (a) DRS, PLE and PL spectra of $Ca_5Ga_6O_{14}$: $0.01Eu^{2+}$ at room temperature. (b) Emission spectra of $Ca_5Ga_6O_{14}$: xEu^{2+} (x = 0-0.02). (c) Emission spectra of $Ca_5Ga_{6-y}Al_yO_{14}$: $0.01Eu^{2+}$ (y =0-0.4). (d) Quantum efficiency measurement of $Ca_5Ga_{6-y}Al_yO_{14}$: $0.01Eu^{2+}$ (y = 0.2). (e) Diff use reflection spectrum of $Ca_5Ga_{6-y}Al_yO_{14}$: $0.01Eu^{2+}$ (y = 0-0.4). (f) Blue light absorption of $Ca_5Ga_{6-y}Al_yO_{14}$:$0.01Eu^{2+}$ (y = 0-0.4).

the Eu doping concentration gradually increases, the emission intensity exhibits an initial rise followed by a decrease. Initially, higher doping concentrations enhance luminescence intensity by increasing the number of emission centers. However, when the doping concentration exceeds the optimal level, the interionic spacing decreases, leading to enhanced interactions between adjacent ions. Cross-relaxation between energy levels becomes more probable, resulting in concentration quenching and diminished luminescence brightness. At $Ca_5Ga_6O_{14}$: $0.01Eu^{2+}$ exhibits the strongest luminescence intensity, making this sample the optimal choice for subsequent experimental testing.

The quantum efficiency of phosphors is a critical parameter for their applicability in white light LEDs. The quantum efficiency of $Ca_5Ga_6O_{14}$: $0.01Eu^{2+}$ excited at 468 nm was measured, as shown in Fig. S5, with a quantum efficiency of 17.61%. Clearly, this low quantum efficiency poses a significant barrier to its application in white LEDs. Therefore, enhancing the quantum efficiency of $Ca_5Ga_6O_{14}$: $0.01Eu^{2+}$ phosphor is essential to better align with the application requirements for solid-state lighting. We adopted a strategy of ion substitution to alter the local crystal field environment, aiming to improve quantum efficiency. Here, we selected Al^{3+}, a homologous group element, to substitute Ga^{3+} in the host lattice. As its identical +3 valence ensures charge-neutral isovalent doping, well-matched ionic radius enables stable lattice incorporation without impurity formation, and stronger Al-O bonds enhance host lattice rigidity to suppress non-radiative transitions, all of which are favorable for boosting the luminescence efficiency of the phosphor. To investigate the effect of Al^{3+} substitution on the phosphor′s luminescence properties, the emission spectrum of $Ca_5Ga_{6-y}AlyO14$: $0.01Eu^{2+}$ (y = 0-0.4) was measured upon 468 nm excitation, as shown in Fig. 2c. The $4f^7 \rightarrow 4f^65d^1$ electronic transition is parity-allowed [24]. Due to the 5d orbital′s sensitivity to the surrounding lattice environment, the Eu^{2+} 4f-5d transition exhibits broad absorption and emission bands[25]. As the Al^{3+} substitution concentration increases, the phosphor emission intensity first rises and then decreases. At an Al^{3+} concentration of 0.2, the emission intensity of $Ca_5Ga_{6-y}Al_yO_{14}$: $0.01Eu^{2+}$ reaches its maximum, with a measured quantum efficiency of 79.2%, as shown in Fig. 2d.

To investigate the reasons for increased light intensity and quantum efficiency, diffuse reflectance spectra were measured for $Ca_5Ga_{6-y}Al_yO_{14}$: $0.01Eu^{2+}$ (y = 0-0.4), as shown in Fig. 2e. Its DRS absorption band corresponds well with the excitation spectrum, exhibiting an absorption band in the 400-600 nm range that matches the emission band of the blue light chip. The DRS spectra demonstrate that the introduction of Al^{3+} modulates the light absorption capability of the material. As the Al^{3+} substitution concentration increases, the blue light absorption of the material first rises and then diminishes, as shown in Fig. 2f. This trend aligns with the light intensity trend depicted in Fig. 2c. At an Al^{3+} concentration of 0.2, the highest diffuse reflectance indicates the strongest absorption, with a measured quantum efficiency of 79.2%, representing a significant improvement over the undoped state. The blue light absorption capacity of phosphors primarily depends on the center-of-mass shift and the degree of crystal field splitting [26, 27]. In $Ca_5Ga_{6-y}Al_yO_{14}$: $0.01Eu^{2+}$ (y = 0-0.4), the covalent nature of bonds with Eu^{2+} ions remains unchanged, and the shift in the center of mass has little effect on the excitation band of the material. Therefore, the variation in blue-light absorption of the material is primarily attributed to changes in crystal field splitting degree. During Al^{3+} substitution, since the ionic radius of Al^{3+} (0.535 Å) is smaller than that of Ga^{3+} (0.62 Å), partial replacement of Ga^{3+} by Al^{3+} induces lattice contraction, enhancing the crystal field strength around Eu^{2+}. This slight increase in crystal field strength can still alter the vibrational coupling state of energy levels, leading to enhanced blue light absorption[28].

The bandgap of the sample can be calculated using the Kubelka-Munk equation[29]:

$$F(R) = \frac{(1-R)^2}{2R} \# (1)$$

$$Ah\nu = c\left(h\nu - E_g\right)^{\frac{1}{2}} \#(2)$$

$$\left[h\nu F\left(R_\infty\right)\right]^2 = A\left(h\nu - E_g\right) \#(3)$$

Here, R denotes the reflection coefficient, hν represents the photon energy, c is the absorption constant, and E_g signifies the optical bandgap. As shown in Fig. S6 (a) and (b), based on the relationship between $[F(R_\infty)\ h\nu]^{1/2}$ and 1240/λ for $Ca_5Ga_6O_{14}$: 0.01$Eu^{2+}$and $Ca_5Ga_{6-y}Al_yO_{14}$: 0.01Eu^{2+} (y = 0.2), the relationship between $[F(R_\infty)\ h\nu]^{1/2}$ and 1240/λ reveals bandgaps of 2.01 eV and 2.14 eV, respectively. This demonstrates that partial substitution of Ga^{3+} ions by Al^{3+} ions broadens the phosphor bandgap. The increase in material bandgap width confirms lattice contraction[30], which occurs because lattice contraction reduces interatomic distances and enhances electron orbital overlap[31].

The operating temperature of phosphor-converted white LEDs typically reaches around 423 K, with the temperature stability of phosphors limiting their application potential[32]. Thermal quenching behavior is commonly caused by factors such as thermal ionization, thermal relaxation, and crystal rigidity. To better understand the temperature-dependent luminescence characteristics of this sample, temperature-dependent emission spectra of $Ca_5Ga_6O_{14}$: 0.01Eu^{2+} and $Ca_5Ga_{6-y}Al_yO_{14}$: 0.01Eu^{2+} (y=0.2)were measured from room temperature 298 K to 423 K and above, with a step of 25 K, as shown in Fig. 3a and Fig. 3b. Following Al^{3+}substitution for Ga^{3+}, the thermal quenching effect in the samples markedly diminished, and thermal stability improved. As temperature increased, the luminescence intensity of the samples gradually decreased. Fig. 3c shows the temperature dependence of the normalized emission intensities for $Ca_5Ga_6O_{14}$:0.01Eu^{2+} and $Ca_5Ga_{6-y}AlyO$ 14: 0.01Eu^{2+} (y=0.2). At the white LED operating temperature of 423 K, the intensity of $Ca_5Ga_6O_{14}$: 0.01Eu^{2+} is 22% of its room temperature intensity. Following Ga substitution with Al, the sample's intensity at 423 K reached 60% of its value at room temperature. Upon further heating to 473 K,

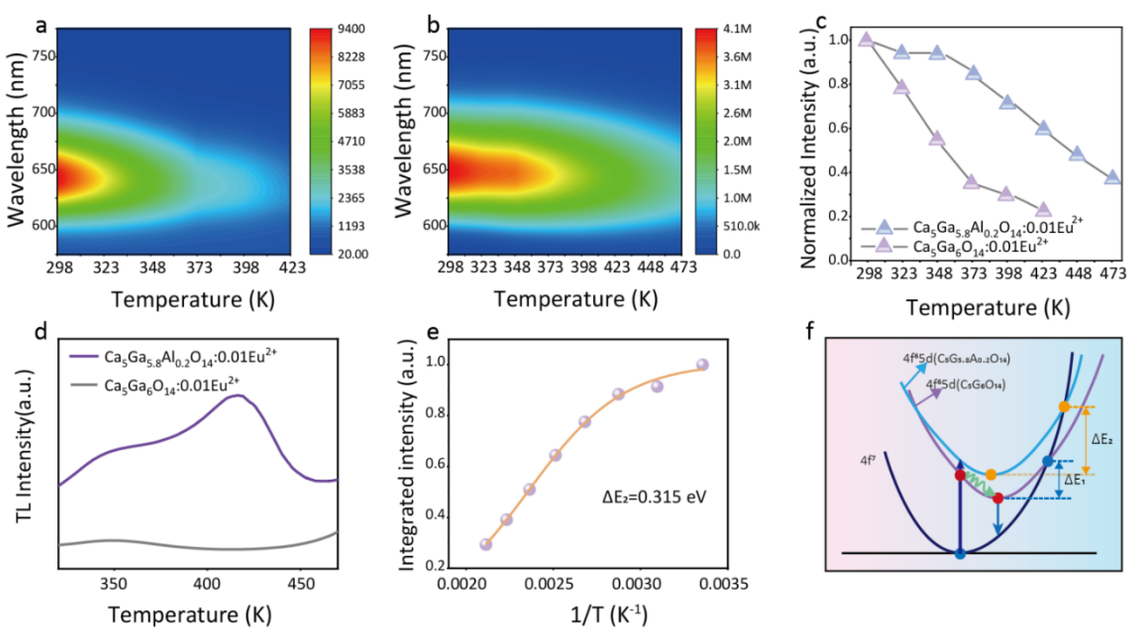

图 3 (a) 298-423 K下Ca5Ga6O14: 0.01Eu2+的温度依赖性光谱;(b)298-473 K下Ca5Ga6-yAlyO14:0.01Eu2+ (y = 0.2)的温度依赖性光谱;(c) Ca5Ga6O14: 0.01Eu2+和Ca5Ga6-yAlyO14:0.01Eu2+ (y = 0.2)荧光粉的归一化热猝灭特性;(d)热释光谱;(e) $Ca_5Ga_{6-y}Al_yO_{14}$:0.01Eu^{2+} (y = 0.2)的拟合活化能图;(f) $Ca_5Ga_6O_{14}$: 0.01Eu^{2+} 和 $Ca_5Ga_{6-y}Al_yO_{14}$: 0.01Eu^{2+}的热猝灭机制。

Fig.3 (a) Temperature dependence emission spectra of $Ca_5Ga_6O_{14}$:0.01Eu^{2+} (298-423 K).(b)Temperature dependence emission spectra of $Ca_5Ga_{6-y}Al_yO_{14}$:0.01Eu^{2+} (y = 0.2). (c) Normalized thermal quenching behavior of $Ca_5Ga_6O_{14}$: 0.01Eu^{2+} and $Ca_5Ga_{6-y}Al_yO_{14}$:0.01Eu^{2+} (y = 0.2). (d) TL spectra. (e) Fitted activation energy diagram for $Ca_5Ga_{6-y}Al_yO_{14}$:0.01Eu^{2+} (y = 0.2). (f) Mechanism of thermal quenching of $Ca_5Ga_6O_{14}$: 0.01Eu^{2+} and $Ca_5Ga_{6-y}Al_yO_{14}$:0.01Eu^{2+}.

$Ca_5Ga_{6-y}Al_yO_{14}$: 0.01Eu^{2+} (y=0.2) exhibited 37% of its room-temperature intensity, demonstrating strong thermal quenching resistance due to the effective suppression of non-radiative transitions. The superior luminescence properties of $Ca_5Ga_{6-y}Al_yO_{14}$: 0.01Eu^{2+} (y=0.2) form the basis for its potential application in white light LEDs.

To deeply elucidate the intrinsic mechanism of the improved luminescence and thermal stability of the phosphor after Al^{3+} substitution, thermoluminescence (TL) spectra of the series of samples were characterized to analyze the trap structure and carrier capture behavior of the materials. Since the ionic radius of Al^{3+} is smaller than that of Ga^{3+} in the $Ca_5Ga_6O_{14}$ host lattice, lattice distortion changes and slight lattice contraction occur due to variations in the average ionic radius r when Al^{3+} is doped to replace Ga^{3+}[33]. Furthermore, cation disorder can form deep-level trap defects, which serve as electron capture centers in the conduction band, enabling charge level compensation[34]. To quantitatively characterize the depth and density of these trap defects induced by cation disorder, TL spectra were measured over the temperature range from 298 K to 473 K, as shown in Fig. 3d. The trap depth E_T can be calculated using the following formula:

$$E_T = \frac{T_m}{500} \#(4)$$

The temperature at which maximum intensity occurs, Tm, is expressed in kelvins (K). The E_T values are approximately 0.712 eV and 0.833 eV. Compared to undoped phosphors, phosphors doped with Al^{3+} exhibit a significant increase in both the number and depth of traps. Further clarification is needed regarding the impact of trap depth on thermal quenching[35]. At room temperature, the electrons of Eu^{2+} are excited from the 4f ground state to the 5d excited state. A portion of these excited electrons is then ionized into the conduction band (CB) and subsequently captured by shallow or deep traps. As temperature increases, non-radiative transitions dominate the decay process in $Ca_5Ga_6O_{14}$:0.01Eu^{2+}, resulting in poor thermal stability. Conversely, for $Ca_5Ga_{6-y}Al_yO_{14}$: 0.01Eu^{2+} (y = 0.2), cation disorder generates additional deep traps , electrons excited in this system are captured by deep traps. This process compensates for more electrons during emission, thereby reducing nonradiative transitions and enhancing thermal quenching resistance.

Activation energy is commonly used to describe the ease or difficulty of chemical reactions or physical processes[36]. The thermal quenching activation energy ΔE represents the energy barrier that excited-state electrons must overcome to transition from radiative to non-radiative processes. At lower temperatures, excited electrons primarily return to the ground state via radiative transitions[37]. As temperature increases, these excited electrons become more likely to overcome the ΔE energy barrier, triggering non-radiative transitions and consequently reducing luminescence intensity. Therefore, ΔE serves as a key indicator of thermal stability; a higher ΔE value makes it more difficult for electrons to overcome the non-radiative transition barrier, thereby enhancing radiative emission [23, 38]. Temperature stability is closely related to activation energy, where high activation energy typically indicates superior thermal stability in materials. Activation energy (ΔE) can be obtained using the Arrhenius equation:

$$I = I_0\left[1 + Aexp\left(-\frac{\Delta E}{KT}\right)\right]^{-1} \#(5)$$

Here, k is the Boltzmann constant, c is the pre-exponential coefficient, ΔE is the activation energy, and I_T and I_0 are the integrated intensities at a specific temperature and room temperature, respectively. Fitting reveals an activation energy of 0.315 eV for $Ca_5Ga_{6-y}AlyO_{14}$: 0.01Eu^{2+} (y = 0.2), with fitting results shown in Fig. 3e. The superior luminescent properties of $Ca_5Ga_{6-y}Al_yO_{14}$: 0.01Eu^{2+} (y = 0.2) form the basis for its potential application in white light LEDs. Considering that thermal quenching behavior is closely related to non-radiative transitions in electron-phonon interactions, schematic diagram of the thermal quenching mechanism is further provided, as shown in Fig. 3f. As temperature increases, excited electrons must reach the intersection point with the ground state to release phonons and return to the ground state via non-radia-

tive transitions, thereby generating thermal quenching [39, 40]. When excited by 468 nm light, electrons in the ground state $4f^7$ can transition to the excited state 5d via pathway 1. The excited electrons relax to the equilibrium position (point C) through the lattice via pathway 2, then return to the $4f^7$ ground state via pathway 3, resulting in 650 nm red light emission. During this process, electrons reach the equilibrium position through lattice relaxation. As temperature increases, electrons in the excited state couple with thermally activated phonons. The energy of these excited electrons can then reach the intersection point of the 4f and 5d curves, allowing them to return to the ground state. Higher activation energy makes it more difficult for electrons to overcome the energy barrier for non-radiative transitions, increasing the likelihood of returning to the ground state via radiative transitions and enhancing thermal stability. Calculations indicate that the ΔE_1 value for $Ca_5Ga_6O_{14}:0.01Eu^{2+}$ is 0.261 eV lower than that for $Ca_5Ga_{6-y}Al_yO_{14}:0.01Eu^{2+}$ (y = 0.2), as shown in Fig. S7. This suggests that partial substitution of Ga^{3+} with Al^{3+} enhances the sample's resistance to thermal quenching.

3.3 Application

Under blue light chip excitation, the $Ca_5Ga_{6-y}Al_yO_{14}:0.01Eu^{2+}$ (y=0.2) red phosphor exhibits potential for achieving high color rendering index when applied as a red phosphor in white LEDs. To validate the practical application value of $Ca_5Ga_{6-y}Al_yO_{14}:0.01Eu^{2+}$ (y=0.2), this red phosphor was combined with commercial yellow-green phosphor $Y_3(Al,Ga)_5O_{12}:Ce^{3+}$ and blue InGaN chips to fabricate white LED devices. Fig. 4a shows the electroluminescence spectrum of the packaged white LED. It is evident that $Ca_5Ga_{6-y}Al_yO_{14}:0.01Eu^{2+}$(y=0.2) effectively compensates for the red deficiency in the full

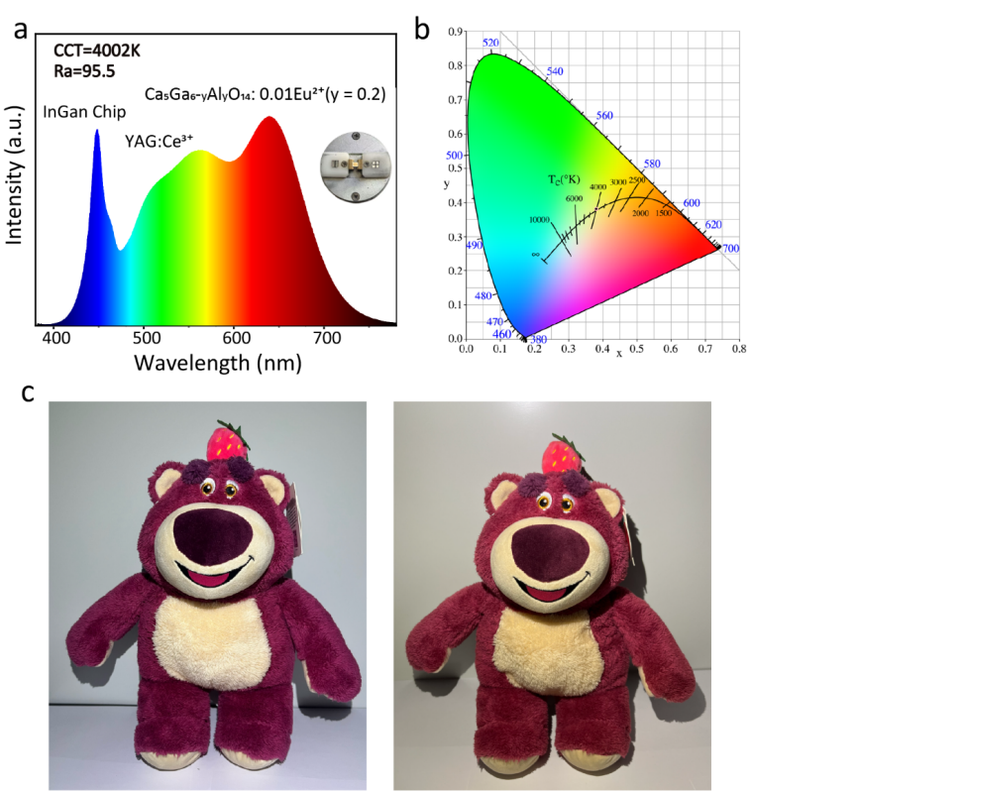

图4 (a) 白光LED(蓝光芯片+YAG: Ce3++Ca5Ga5.8Al0.2O14: 0.01Eu2+)的电致光谱;(b)白光LED器件的色度坐标图;(c)在不同白光LED照明下的玩偶对比图(图左侧为蓝光芯片与YAG: Ce3+;图右侧为蓝光芯片与YAG: Ce3+以及Ca5Ga5.8Al0.2O14: 0.01Eu2+。

Fig.4 (a) Electroluminescence spectrum of white light LED blue light chip + YAG: Ce^{3+}+$Ca_5Ga_{5.8}Al_{0.2}O_{14}:0.01Eu^{2+}$ (y = 0.2). (b) CIE chromaticity diagram. (c) Comparison of dolls under different white LED lighting (The left side of the figure shows the blue light chip and YAG: Ce^{3+}, The right side of the figure shows the blue light chip with YAG: Ce^{3+} and $Ca_5Ga_{5.8}Al_{0.2}O_{14}:0.01Eu^{2+}$.

spectrum. This white LED exhibits a high color rendering index of 95.5 and a low correlated color temperature of 4002 K. Fig. 4b displays the CIE coordinates of the fabricated white LED at (0.3816, 0.3813), positioned within the white light region. Fig. 4c compares photographs of physical objects illuminated by the two white LED light sources. The left image in Fig. 4c shows an object illuminated by a white LED using a blue chip and commercial YAG: Ce^{3+} phosphor. The higher color temperature and greater blue light component result in a cool white appearance in the photograph. The right image in Fig. 4c shows an object photographed under illumination from a white LED using a blue light chip, commercial yellow-green phosphor, and $Ca_5Ga_{6-y}Al_yO_{14}$:0.01Eu^{2+} (y=0.2)red phosphor. The reduced blue light component in this white light results in a warm-toned appearance. In contrast, this white LED achieves warm white illumination while maintaining a high color rendering index, significantly enhancing the quality of life for users.

4 Conclusions

A red phosphor $Ca_5Ga_6O_{14}$:Eu^{2+} with a longer emission wavelength was synthesized via the high-temperature solid-state method. Excited by 468 nm blue light, the phosphor exhibits a luminescence center at 650 nm, with an emission range spanning 550-800 nm. Through the substitution of Ga^{3+} ions via Al^{3+} ions, the structural rigidity of thehost lattice was enhanced, thus improving the thermal stability of the phosphor. Combined with diffuse reflectance spectroscopy analysis, this cation-tuning strategy strengthened Eu^{2+} blue light absorption capability, thereby increasing the phosphor′s quantum efficiency from 17.61% to 79.2%. When paired with a commercial yellow-green phosphor $Y_3(Al, Ga)_5O_{12}$: Ce^{3+} and a blue light chip, the white LED achieved a color rendering index (CRI) of 95.5 and a correlated color temperature (CCT) of 4002 K, delivering high-CRI warm white illumination.

References:

[1] 章伟, 何梦婷, 乔旭升, 等. Mn^{4+}激活的典型LED红色荧光粉研究进展[J]. 发光学报, 2021, 42(9): 1345-1364.
ZHANG W, HE M T, QIAO X S, *et al*. Research Progress of Mn^{4+} Activated Typical LED Red Phosphors [J]. *Chin. J. Lumin.*, 2021, 42(9):1345-1364. (in Chinese)

[2] YAO Q, HU P, SUN P, *et al*. YAG:Ce^{3+} Transparent Ceramic Phosphors Brighten the Next-Generation Laser-Driven Lighting [J]. *Adv. Mater.*, 2020, 32(19):1907888.

[3] 武文杰, 阿木古楞, 刘文全, 等. 氮(氧)化物荧光粉的合成与发光性能[J]. 液晶与显示, 2017, 32(09): 663-676.
WU W J, AMUGULEN, LIU W Q, *et al*. Synthesis and luminescence of nitride and oxynitride luminescent materials [J]. *Chinese Journal of Liquid Crystals and Displays*, 2017, 32(09):663-676. (in Chinese)

[4] 魏东, 苏文霞. 白光LEDs用掺杂Eu^{2+}和Mn^{2+}的$CaAlSiN_3$荧光粉合成及发光性能改进[J]. 发光学报, 2024, 45(10): 1656-1666.
WEI D, SU W X. Synthesis and Luminescence Improvement of $CaAlSiN_3$ Phosphors Doped with Eu^{2+} and Mn^{2+} for White LEDs [J]. *Chin. J. Lumin.*, 2024, 45(10):1656-1666. (in Chinese)

[5] WANG Y, WANG Y, WANG M, *et al*. Facile preparation and formation mechanism of $Sr_2Si_5N_8$:Eu^{2+} red-emitting phosphors [J]. *Mater. Res. Express*, 2018, 5(5):056202.

[6] CHEN J, ZHAO W, FANG Y, *et al*. Continuous production of K_2SiF_6:Mn^{4+} red phosphor by green route synthesis method for warm WLEDs application [J]. *Opt. Mater.*, 2022:112781.

[7] LIU X L, SONG Z, WANG S X, *et al*. The red persistent luminescence of (Sr, Ca)$AlSiN_3$:$Eu^{2+}$and mechanism different to $SrAl_2O_4$:Eu^{2+}, Dy^{3+} [J]. *J. Lumin.*, 2019, 208:313-321.

[8] HU T, GAO Y, MOLOKEEV M S, *et al*. Eu^{2+} Stabilized at Octahedrally Coordinated Ln^{3+} Site Enabling Red Emission in $Sr_3LnAl_2O_{7.5}$ (Ln = Y or Lu) Phosphors [J]. *Adv. Opt. Mater.*, 2021, 9(9):2100077.

[9] GU X, HE Z, SUN X Y. Broadband red emission in disordered Sr_2LaGaO_5:Eu^{2+} phosphors [J]. *Chem. Phys.*, 2024, 589:112514.

[10] 郑飞, 茅云蔚, 杨波波, 等. 基于YAG:Ce^{3+}荧光粉复合Eu^{3+}掺杂荧光玻璃的激光照明器件[J]. 发光学报, 2019, 40(7): 842-848.
ZHENG F, MAO Y W, YANG B B, *et al.* Laser Lighting Device Based on YAG: Ce^{3+} Phosphor Composite Eu^{3+} Doped Phosphor-in-glasses [J]. *Chin. J. Lumin.*, 2019, 40(7):842-848. (in Chinese)

[11] YANG Z, ZHOU Y, QIAO J, *et al.* Rapid Synthesis of Red-Emitting $Sr_2Sc_{0.5}Ga_{1.5}O_5:Eu^{2+}$ Phosphors and the Tunable Photoluminescence Via Sr/Ba Substitution [J]. *Adv. Opt. Mater.*, 2021, 9(16):2100131.

[12] ZHAO Q R, WANG Y L, DUAN T Z, *et al.* Blue-light-excited red emission in a CaO:Eu phosphor [J]. *J. Lumin.*, 2022, 253:119457.

[13] LI X J, LI P L, FENG X X, *et al.* Achievement of high photoluminescence quantum yield orange-red phosphors by designing Eu^{2+} reduction environment for multi applications [J]. *Ceram. Int.*, 2023, 50(7):10278-10284.

[14] HU T, JIANG Z L, WANG B, *et al.* Eu^{2+} luminescence in $CaYGaO_4$ olivine: a new efficient red phosphor for warm illumination [J]. *J. Mater. Chem. C*, 2023, 11(6):2153-2161.

[15] 管鹤群, 崔俊, 刘丽丽, 等. LuAG:Ce荧光粉的熔盐法制备及其发光性能研究[J]. 中国稀土学报, 2019, 37(5): 537-544.
GUAN H Q, CUI J, LIU L L, *et al.* Molten Salt Synthesis and Luminescence Properties of LuAG:Ce Phosphor [J]. *J. Chin. Soc. Rare Earths*, 2019, 37(5):537-544. (in Chinese)

[16] 邝宇航, 朱英泽, 夏志国. 氧化物红色荧光粉$Sr_3Ga_4O_9:Eu^{2+}$中Eu^{2+}的格位工程调控机制[J]. 硅酸盐学报, 2024, 52(11): 3482-3491.
KUANG Y H, ZHU Y Z, XIA Z G. 氧化物红色荧光粉$Sr_3Ga_4O_9:Eu^{2+}$中Eu^{2+}的格位工程调控机制[J]. *J. Chin. Ceram. Soc.*, 2024, 52(11):3482-3491. (in Chinese)

[17] 张家骅, 吕伟, 郝振东, 等. 利用能量传递实现可调全色单一白光$BaMg_2Al_6Si_9O_{30}:Eu^{2+},Tb^{3+},Mn^{2+}$荧光粉(特邀)[J]. 中国光学, 2012, 5(03): 203-208.
ZHANG J H, LV W, HAO Z D, *et al.* Color-tunable white-light emitting $BaMg_2Al_6Si_9O_{30}:Eu^{2+},Tb^{3+},Mn^{2+}$ phosphors via energy transfer(Invited) [J]. *Chinese Optics*, 2012, 5(03):203-208. (in Chinese)

[18] POORT S H M, BLOKPOEL W P, BLASSE G. Luminescence of Eu^{2+} in barium and strontium aluminate and gallate [J]. *Chem. Mater.*, 1995, 7(8):1547-1551.

[19] LI N, ZHANG P F, WANG Z Q, *et al.* Novel UV and X-ray irradiated white-emitting persistent luminescence and traps distribution of $Ca_5Ga_6O_{14}:Pr^{3+}$ phosphors [J]. *J. Alloys Compd.*, 2021, 858:157719.

[20] LIU Z C, SHEN C Y, YUAN L, *et al.* $Ca_5Ga_6O_{14}:Eu^{3+}$: A novel phosphor with outstanding heat resistance for white light-emitting diodes [J]. *J. Am. Ceram. Soc.*, 2019, 102(7):3823-3828.

[21] ZHANG Y, LI R, PENG X, *et al.* Photoluminescence modulation of red-emitting $Sr_2ScGaO_5:Eu^{2+}$ phosphor via cation substitution for WLED and fingerprint identification [J]. *J. Alloys Compd.*, 2025:185287.

[22] LI Y, WANG N, YANG L, *et al.* High-temperature-stable $Sr_3GaAlO_6:Eu^{2+}$ broadband red phosphor: Dual applications from LED lighting to fingerprint development [J]. *Ceram. Int.*, 2026,

[23] YANG Z Y, ZHAO Y F, ZHOU Y Y, *et al.* Giant Red-Shifted Emission in $(Sr,Ba)Y_2O_4:Eu^{2+}$ Phosphor Toward Broadband Near-Infrared Luminescence [J]. *Adv. Funct. Mater.*, 2021, 32(1):2103927.

[24] KIM K-H, KANG E-H, KANG B-K, *et al.* Synthesis of $SrLu_2O_4:Eu^{2+}$ red phosphors and their photoluminescence properties [J]. *J. Lumin.*, 2017, 183:13-16.

[25] 王凯旋, 周雪莲, 张钰, 等. 高效率$BaAl_4Sb_2O_{12}:Eu^{2+}$荧光粉合成与发光性能[J]. 发光学报, 2024, 45(05): 753-761.
XUAN W K, ZHOU X L, ZHANG Y, *et al.* Synthesis and Luminescent Properties of High Brightness $BaAl_4Sb_2O_{12}:Eu^{2+}$ Phosphors [J]. *Chin. J. Lumin.*, 2024, 45(05):753-761. (in Chinese)

[26] HUO X, WANG Z, MENG X, *et al.* Structure tailoring and defect engineering of a highly thermally stable red emitting phosphor [J]. *J. Mater. Chem. C*, 2024, 12(12):4287-4295.

[27] ZHAO J T, SUN X Y, WANG Z Q. Ce^{3+}/Eu^{2+} doped $SrSc_2O_4$ phosphors: synthesis, luminescence and energy transfer from Ce^{3+} to Eu^{2+} [J]. *Chem. Phys. Lett.*, 2017, 691:68-72.

[28] ZHANG X W, SUN D S, LU Z, *et al.* Engineering Broadband Emission of $Zn_2Ga_{0.5}$-$yAl_ySb_{0.5}O_4:Cr^{3+}$ Phosphors for Near-Infrared LED Application [J]. *Small*, 2025, 21(25):2503049.

[29] XIANG J M, ZHENG J M, ZHAO X Q, *et al*. Synthesis of broadband NIR garnet phosphor $Ca_4ZrGe_3O_{12}$: Cr^{3+}, Yb^{3+} for NIR pc-LED applications [J]. *Mater. Chem. Front.*, 2022, 6(4): 440-449.

[30] JI X Y, ZHANG J L, LI Y, *et al*. Improving Quantum Efficiency and Thermal Stability in Blue-Emitting $Ba_{2-x}Sr_xSiO_4$: Ce^{3+} Phosphor via Solid Solution [J]. *Chem. Mater.*, 2018, 30(15): 5137-5147.

[31] WANG B, CHEN Z K, LI X S, *et al*. Photostimulated near-infrared persistent luminescence Cr^{3+}-doped Zn-Ga-Ge-O phosphor with high QE for optical information storage [J]. *J. Alloys Compd.*, 2020, 812: 152119.

[32] DONG Q Z, ZHANG W B, TIAN B L, *et al*. Controlling defects to improve the emission intensity of $NaMgBO_3$: 1%Ce^{3+} blue-cyan phosphor [J]. *J. Mater. Sci.: Mater. Electron.*, 2022, 33(19): 15604-15616.

[33] WANG Y H, DING J Y, WANG Y C, *et al*. Structural design of new Ce^{3+}/Eu^{2+}-doped or co-doped phosphors with excellent thermal stabilities for WLEDs [J]. *J. Mater. Chem. C*, 2019, 7(7): 1792-1820.

[34] ZHANG T F, ZHANG D, GAO Z Y, *et al*. Enhanced quantum efficiency and thermal stability of cyan-green emitting Ba-$Lu_2Al_3ScGeO_{12}$: Ce^{3+}, Si^{4+} phosphor via cation substitution for WLEDs [J]. *J. Alloys Compd.*, 2025, 1032: 181133.

[35] 杨椿洋, 孙晓园, 谭琴琴, 等. 具有优异热稳定性的 $CaLa_{0.5}Y_{0.5}AlO_4$:Sm^{3+}荧光粉制备及发光特性 [J]. 发光学报, 2026, 47(1): 104-113.
YANG C Y, SUN X Y, TAN Q Q, *et al*. Synthesis and Luminescence Properties of $CaLa_{0.5}Y_{0.5}AlO_4$:Sm^{3+} Phosphors with Excellent Thermal Stability [J]. *Chin. J. Lumin.*, 2026, 47(1): 104-113. (in Chinese)

[36] MEI J, LV L M, GAO J S, *et al*. Luminescence and thermal stability tuning in $(Ba,Mn)_3(Gd,Y)Na(PO_4)_5F$:$Eu^{2+}$ phosphors via cation-substitution [J]. *Opt. Mater.*, 2018, 78: 452-456.

[37] LIU H M, LIANG H W, ZHANG W Y, *et al*. Improving the thermal stability and luminescent efficiency of $(Ba,Sr)_3SiO_5$: Eu^{2+} phosphors by structure, bandgap engineering and soft chemistry synthesis method [J]. *Chem. Eng. J.*, 2021, 410: 128367.

[38] ZHU Y Z, WANG X S, QIAO J W, *et al*. Regulating Eu^{2+} Multisite Occupation through Structural Disorder toward Broadband Near-Infrared Emission [J]. *Chem. Mater.*, 2023, 35(3): 1432-1439.

[39] HE C, TAKEDA T, HUANG Z H, *et al*. Powder Synthesis and Luminescence of a Novel Yellow-emitting $Ba_5Si_{11}Al_7N_{25}$: Eu^{2+} Phosphor Discovered by a Single-particle-diagnosis Approach for Warm w-LEDs [J]. *Chem. Eng. J.*, 2022, 455: 140932.

[40] DENAULT K A, BRGOCH J, GAULTOIS M W, *et al*. Consequences of Optimal Bond Valence on Structural Rigidity and Improved Luminescence Properties in $Sr_xBa_{2-x}SiO_4$:Eu^{2+} Orthosilicate Phosphors [J]. *Chem. Mater.*, 2014, 26(7): 2275-2282.

康梦伊(2002-),女,河北邢台人,硕士研究生,2024年于河北大学获得学士学位,主要从事发光材料及其应用方面的研究。
E-mail: 1683632163@qq.com

李盼来(1978-),男,河北河间人,博士,教授,博士生导师,2014年于北京交通大学获得博士学位,主要从事发光材料及其应用方面的研究。
E-mail: li_panlai@126.com

王志军(1979-),女,河北沧州人,博士,教授,博士生导师,2016年于北京交通大学获得博士学位,主要从事发光材料及其应用方面的研究。
E-mail: wangzj1998@126.com